The hypersonic viscous effect on a flat plate with finite leading edge

By ANDREW G. HAMMITT
Princeton University, Princeton, New Jersey

(Received 6 June 1958)

A method has been developed for calculating the viscous effects of the hypersonic flow on the fore part of various bodies. This method takes into account the finite leading-edge thickness of the body and the detached shock wave. The calculated pressure distributions agree with all experimental results for both air and helium over a wide range of Mach numbers and Reynolds numbers. The calculation predicts skin frictions of the order of twice those predicted by ordinary boundary-layer theory.

1. Introduction

The flow about the leading edge of a flat plate at hypersonic speeds has been considered in several theoretical and experimental studies. The first mention of the problem in the literature is by Becker (1950). In some experiments made in the N.A.C.A. hypersonic tunnel at Langley Field, it was observed that the pressure on the forward surface of a wedge-shaped airfoil was not constant as predicted by classical inviscid flow theory, and was above the indicated value near the leading edge. It was suggested that the growth of the boundary layer on the surface created an effectively curved surface, and rough calculations showed that this mechanism seemed to account for the observed results.

Following this initial work, several authors published analytical papers in which they attempted to calculate the flow field caused by the interaction of the viscous boundary layer with the inviscid flow behind the shock wave. These papers attacked the problem in two ways: the first method, used by Shen (1952), Li & Nagamatsu (1953, 1955) and Pai (1953), treated the whole flow region between the shock wave and the plate by the boundary-layer equations; and the second method, adopted by Bertram (1952) and Lees (1952, 1954*a*, *b*), followed the suggestion by Becker of dividing the region between shock wave and the wall into inviscid and viscous regions. Bogdonoff & Hammitt (1956) pointed out that there were some basic inconsistencies in the first method which did not exist in the second. Both approaches predicted about the same pressure distributions over flat plates.

Experimental studies of the flow over flat plates, made by Bogdonoff & Hammitt (1956) in the helium hypersonic wind tunnel at Princeton University at Mach numbers between 11 and 15, showed that the pressures on the surface were considerably higher than those predicted by the various analytical methods previously mentioned. In later experimental work (Hammitt, Vas & Bogdonoff

1956; Hammitt & Bogdonoff 1956), it was found that the leading-edge thickness t had an important influence on the surface pressures and that for the higher Reynolds numbers based on t the results depended only on x/t, where x is the distance along the plate from the leading edge. This result led to the conclusion that the pressures on the plate were caused by the inviscid flow field behind the finite leading edge and were independent of the viscous effects of the boundary layer growth. This inviscid part of the flow field seems to be important for very thin leading edges. Since such an effect was not included in the theories for infinitely thin leading edges, the results are not applicable when the leading-edge Reynolds number is greater than 100 for distances from the leading edge up to $10{,}000x/t$.

Other experimental work by Kendall (1957), carried out in air tunnels at Mach numbers of the order of 6, does not show this large dependence on leading-edge thickness, and the experimental pressure distributions agree with the viscous theories fairly well. The indications are that the inviscid effect of the leading edge decreases more rapidly with Mach number than the viscous effect. Hence, the inviscid part of the leading-edge problem may be unimportant at lower Mach numbers, but may predominate at higher Mach numbers.

In the present report, experimental pressure distributions near the leading edge of flat plates are presented for a wide range of leading-edge Reynolds numbers. An analytical treatment is then presented to account for the Reynolds number dependence of these surface pressures.

2. Experimental studies

A detailed description of the Princeton helium hypersonic tunnel has been given previously by Bogdonoff & Hammitt (1954). This tunnel, using helium as the working fluid, is capable of operating at Mach numbers up to 20, and Reynolds numbers between 0·5 and 2·0 million per inch. An axially symmetric conical nozzle with an 0·2 in. throat and a 3·75 in. working section is used. Because the nozzle is not contoured, but conical, there is a continuous Mach number gradient, but no region of uniform Mach number. Tests are conducted in this non-uniform region.

The model used in these experiments is shown in figure 1. It consists of a flat plate with a square leading edge. Pressure orifices are distributed along the surface, being concentrated near the leading edge and spread out farther back. The leading-edge thickness has been measured using a microscope which enables the thickness to be determined to within $0{\cdot}04 \times 10^{-3}$ in. Leading-edge thicknesses between $0{\cdot}12 \times 10^{-3}$ and $4{\cdot}4 \times 10^{-3}$ in. were tested at several Mach numbers and stagnation pressures.

The pressure distributions on the flat surface are shown in figure 2. In this plot, the distance along the surface is expressed in units of the leading-edge thickness. The surface pressure is expressed as the difference between the measured pressure and the pressure at the same point when the model is absent. In this way, a first-order correction is made for the non-uniform pressure in the test section. This pressure gradient due to varying tunnel Mach number is actually small compared with the pressure gradient measured on the surface, so that this first-order correction should be sufficient. Results are presented for a wide range of leading-edge thicknesses at a Mach number of 11·4, measured at the leading edge of the

model. Data for other Mach numbers and more detailed descriptions of these pressure measurements are given by Vas (1957). Since the data for $M = 11{\cdot}4$ are typical, only this one case will be treated in this paper. The results indicate that for the larger leading-edge Reynolds numbers, the pressure distributions are almost independent of Reynolds number, but are dependent at smaller leading-edge Reynolds numbers.

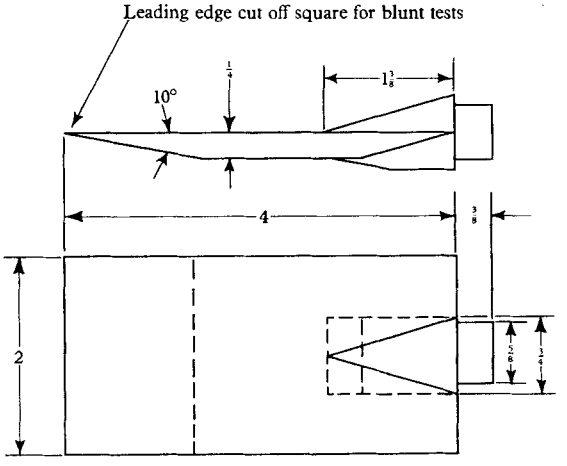

FIGURE 1. Blunted flat plate model used to measure experimental pressure distributions. Dimensions are given in inches.

3. Theory

For a given geometry, the experiments indicate that at high Reynolds numbers the surface pressure distribution is determined by the inviscid flow behind the detached shock wave. At lower Reynolds number, the boundary layer on the body becomes thicker, and modifies the effective body shape, so that the flow field may be described as a flow about the modified body. If this model is correct, the viscous effect can be calculated as the difference between the inviscid flow about the effective body, i.e. the actual body modified by the boundary-layer thickness, and the inviscid flow about the actual body. Through most of the range of Reynolds numbers for which data were presented in figure 2, the viscous effect is a perturbation on the inviscid flow. Therefore a first determination of the viscous effect can be made by calculating the boundary layer in the inviscid flow field and then calculating the modified inviscid flow field about the new effective body shape. A higher order solution may then be determined by using this first-order flow field, and recalculating the boundary layer. As many successive approximations may be made as are required. Because of the difficulty of determining the inviscid flow field behind the detached shock wave, the inviscid solution obtained from the experimental results will be used. This method of solution is essentially the same as was used by Lees & Probstein (1952), except they assumed the inviscid flow field about the body to be uniform and the same as that ahead of the body.

It is interesting to note that, with this method, there are no inherent difficulties at the leading edge. The previous solutions, which assumed an infinitely sharp

leading edge, always introduced a singularity at this point. By recognizing that the leading edge of any real model is always blunt, the present method eliminates this difficulty. The boundary layer grows from the stagnant point solution and no singularity is involved. As the leading edge becomes sharper and the mean free path of the gas molecules becomes of the order of the leading-edge thickness, the flow in this region cannot be treated as a continuum. The model is still correct, but different equations are required to describe the flow.

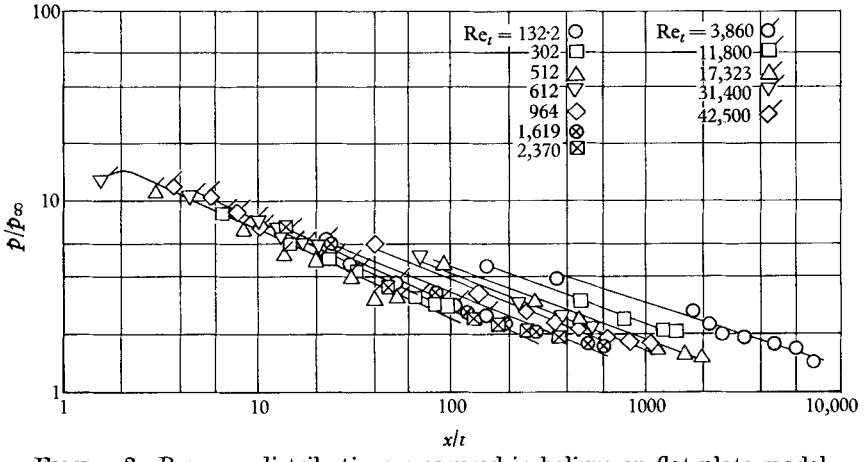

FIGURE 2. Pressure distributions measured in helium on flat plate model for various Re_t; $M = 11{\cdot}1$.

Boundary-layer solution

The zero-order inviscid pressure distribution is taken from the experimental results for the highest Reynolds number. The growth of the boundary layer may be calculated in this flow field by the use of momentum integral techniques. If there were no mass in the boundary layer, the entropy along the outside edge of the boundary layer would always be equal to the value behind the normal shock wave. However, since some flow enters the layer, the entropy at the edge of the boundary layer is continually changing. Far downstream from the leading edge, the entropy will approach the free-stream value, since all of the flow passing through the strong shock wave will be contained in the boundary layer.

The usual equations for the boundary layer are

$$\rho u\frac{\partial u}{\partial x}+\rho v\frac{\partial u}{\partial y}=-\frac{\partial p}{\partial x}+\frac{\partial}{\partial y}\left(\mu\frac{\partial u}{\partial y}\right), \tag{1}$$

$$\frac{\partial(\rho u)}{\partial x}+\frac{\partial(\rho v)}{\partial y}=0, \tag{2}$$

where u, v are the velocity components parallel to x, y, p is pressure, ρ is density and μ is viscosity,

If the equation of motion (1) is integrated in the y-direction (i.e. perpendicular to the plate) between 0 and δ and the continuity equation (2) is used to express the value of v at $y = \delta$, the momentum integral equation is found to be

$$\frac{\partial u_1}{\partial x}\int_0^\delta \rho u\,dy-\frac{d}{dx}\int_0^\delta \rho u(u-u_1)\,dy=\int_0^\delta -\frac{dp_1}{dx}\,dy-\mu_w\left(\frac{\partial u}{\partial y}\right)_{y=0}. \tag{3}$$

In isentropic flow, the pressure can be expressed in terms of the velocity by means of the Bernoulli relation

$$\frac{dp_1}{dx} = -\rho_1 u_1 \frac{du_1}{dx}.$$

When the boundary layer is growing into a region of rotational flow, the entropy changes for each stream line, so the Bernoulli equation cannot be used. In general, for the case of the boundary layer growing in the shock layer behind the highly curved hypersonic shock wave, the relation between pressure and velocity must include the entropy term. In the following development, u_1 and p_1 will be left as independent parameters and will only be related when the entropy on the outside of the boundary layer can be determined.

Let T denote temperature. If the transformation

$$S = \int_0^y \frac{T_1}{T} dy, \quad \delta_S = \int_0^\delta \frac{T_1}{T} dy, \quad \tau = \frac{S}{\delta_S},$$

is introduced, equation (3) reduces to the form

$$-\frac{d}{dx}\rho_1 u_1^2 \delta_S \int_0^1 \left(\frac{u}{u_1} - \frac{u^2}{u_1^2}\right) d\tau + \frac{du_1}{dx}\left[\delta_S \rho_1 u_1 \int_0^1 \frac{u}{u_1} d\tau\right] + \delta_S \frac{dp_1}{dx} \int_0^1 \frac{T}{T_1} d\tau = -\mu_w \frac{u_1 T_1}{T_w \delta_S}\left[\frac{d(u/u_1)}{d\tau}\right]_{\tau=0}. \tag{4}$$

If the viscosity is assumed to follow the law

$$\frac{\mu}{\mu_\infty} = \frac{1}{C}\frac{T}{T_\infty}, \quad \text{where} \quad C = \frac{T_w}{T_\infty}\Big/\frac{\mu_w}{\mu_\infty},$$

and the following quantities are defined

$$F_1 = \int_0^1 \frac{u}{u_1}\left(1 - \frac{u}{u_1}\right) d\tau, \quad F_3 = \left[\frac{\partial}{\partial \tau}\left(\frac{u}{u_1}\right)\right]_{\tau=0},$$

$$F_2 = \int_0^1 \frac{u}{u_1} d\tau, \quad F_4 = \int_0^1 \frac{T}{T_1} d\tau,$$

then

$$\tfrac{1}{2}F_1 \frac{d(\delta S)^2}{dx} + \left[\frac{dF_1}{dx} + F_1 \frac{d(\log \rho_1 u_1^2)}{dx} - F_2 \frac{d(\log u_1)}{dx} - \frac{F_4}{\rho_1 u_1^2}\frac{dp_1}{dx}\right]\delta_S^2 = F_3 \frac{C\mu_\infty}{\rho \mu_1}\frac{T_1}{T_\infty}. \tag{5}$$

Define $\lambda = (\mathrm{Re}_t/C)(\delta_S/t)^2$ and $\zeta = x/t$, where t, the leading-edge thickness, is the characteristic dimension of the problem. Substitution of these quantities in equation (5) gives

$$\lambda' + 2\lambda\left[\frac{F_1'}{F_1} + \frac{\rho_1'}{\rho_1} + \frac{u_1'}{u_1}\left(2 - \frac{F_2}{F_1}\right) - \frac{F_4}{\gamma F_1 M_1^2}\frac{p_1'}{p_1}\right] = 2\frac{F_3}{F_1}\frac{T_1}{T_\infty}\frac{\rho_\infty u_\infty}{\rho_1 \mu_1}, \tag{6}$$

where the primes denote differentiation with respect to ζ. If a power-series representation for the velocity profile is assumed, this equation can be solved in a manner similar to that used by Morduchow & Clarke (1952).

A sixth degree polynomial will be assumed of the form

$$u/u_1 = a_0 + a_1\tau + a_2\tau^2 + a_3\tau^3 + a_4\tau^4 + a_5\tau^5 + a_i\tau^i. \tag{7}$$

The boundary conditions at the inner and outer edges of the boundary layer, expressed in the (x, S)-plane are

$$\tau = 0, \quad \frac{u}{u_1} = 0, \qquad \tau = 1, \quad \frac{u}{u_1} = 1;$$

$$\mu_\infty C \frac{T_1}{T_\infty}\frac{T_1}{T_0}\frac{\partial^2(u/u_1)}{\partial\tau^2} = \frac{1}{u_1}\frac{dp_1}{dx}\delta_S^2, \quad \frac{\partial(u/u_1)}{d\tau} = \frac{\partial^2(u/u_1)}{d\tau^2} = \frac{\partial^3(u/u_1)}{d\tau^3} = 0,$$

$$\partial^3\left(\frac{u}{u_1}\right)\Big/\partial\tau^3 = 0. \tag{8}$$

The second condition at $y = 0$ follows from the original equation of motion (1), and the third condition comes from differentiating equation (1) with respect to y, and adding the condition of zero heat transfer at the wall.

By using the boundary conditions (8), all of the coefficients of equation (7) may be evaluated in terms of one coefficient. If this is done, equation (7) may be written as

$$u/u_1 = 2(1-\tfrac{1}{5}a_2)\tau + a_2\tau^2 - (5+2a_2)\tau^4 + 2(3+a_2)\tau^5 - (2+\tfrac{3}{5}a_2)\tau^6, \tag{9}$$

where

$$a_2 = \frac{\lambda}{2}\left(\frac{T_\infty}{T_1}\right)^2 \frac{T_0}{T_\infty}\frac{u_\infty}{u_1}\frac{1}{\gamma M_\infty^2}\frac{d(p_1/p_\infty)}{d\zeta}.$$

The various integrals used in defining the F's may now be evaluated:

$$F_1 = 0{\cdot}1093 + 0{\cdot}00211a_2 - 0{\cdot}000622a_2^2;$$
$$F_2 = 0{\cdot}7143 - 0{\cdot}01905a_2; \qquad F_4 = 1 + \tfrac{1}{2}(\gamma-1)KM_1^2;$$
$$F_3 = 2 - 0{\cdot}400a_2; \qquad K = 0{\cdot}3950 + 0{\cdot}02116a_2 - 0{\cdot}000622a_2^2.$$

In these equations, a_2, the profile shape parameter, is a function of ζ. In the expressions for F_1, F_2 and F_4, the terms involving a_2 are small, so for boundary layers where a_2 is relatively constant, an average value of a_2 can be used in evaluating these quantities. Equation (6) can then be written

$$\lambda' + 2\lambda\left[\frac{\rho_1'}{\rho} - \frac{u_1'}{u_1}\left(2 - \frac{F_1}{F_2}\right) - \frac{1}{\gamma F_1 M_1^2}\frac{p_1'}{p_1}\left(F_4 - 0{\cdot}2\frac{T_0}{T_1}\right)\right] = \frac{4}{F_1}\frac{u_\infty}{u_1}\frac{\rho_\infty}{\rho_1}\frac{T_1}{T_\infty}. \tag{10}$$

Equation (10) is now a linear differential equation of the first order which may be integrated. In terms of the quantity $G = p_{0_1}/p_{0_\infty}$, which is a measure of the stagnation pressure at the edge of the boundary layer, equation (10) gives

$$\lambda = \frac{4}{F_1}\left[\int_0^\zeta \left\{\frac{1}{G}\left(\frac{u_1}{u_\infty}\right)^a \left(\frac{T_1}{T_\infty}\right)^b G^c e^{-d}\right\} d\zeta\right] \div \left[\left(\frac{u_1}{u_\infty}\right)^{a+1}\left(\frac{T_1}{T_\infty}\right)^{b-1+1/(\gamma-1)} G^c e^{-d}\right],$$

where

$$a = 3 + \frac{2}{F_1}(0{\cdot}08571 + 0{\cdot}01905a_2), \quad b = \frac{\gamma}{\gamma-1} - \frac{K-\frac{1}{5}}{F_1},$$

$$c = 2 - \frac{\gamma-1}{\gamma F_1}(K - \tfrac{1}{5}), \qquad d = \int_0^G \frac{1}{\gamma F_1 M_1^2}\frac{dG}{G}.$$

This equation can be used now to calculate the growth of the boundary layer along an adiabatic wall once p_1, U_1, T_1, M_1 and G are known as a function of ζ.

Inviscid solution

In order to find the inviscid solution, it is necessary to be able to solve the problem of flow behind a detached shock wave. While this problem has received considerable attention, an adequate solution is not available. We are most interested in the flow well downstream from the leading edge, a case treated by Lees & Kubota (1956) and Chang & Pallone (1956). While these studies give results in general agreement with experimental observations, they were found not to be sufficiently accurate, and it was necessary to use empirical results to provide the required information. The pressure field behind the leading edge is affected by expansion waves from the corner which are reflected back into the body either from the sonic line, the entropy discontinuities, or the shock wave, as shown in figure 3. This pressure field can be determined from the experiments with relatively thick leading edges and used as a first approximation for the field at lower Re_t. Data are available for Re_t up to 60×10^3.

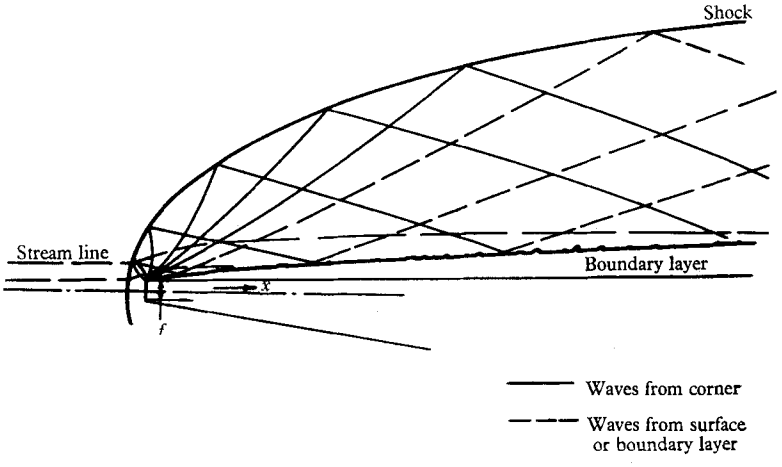

FIGURE 3. Theoretical model illustrating the effect of boundary-layer growth on flow field.

The change in pressure distribution on the plate caused by the boundary layer may be calculated by considering the change in pressure produced by a body of slightly altered contour. If this change is small compared with the value for the unaltered shape, a linearized approximation can be used. For a first approximation, it will be assumed that the boundary condition to be imposed on the inviscid flow is that, on the surface of the plate, the flow deflexion angle is equal to the slope of the effective body shape. The isentropic pressure-angle relation will be used. If this is written in the form of a series,

$$\frac{\Delta p}{p_{\mathrm{in}}} = \frac{\gamma M_1^2}{(M_1^2-1)^{\frac{1}{2}}}\theta + \frac{\gamma(\gamma+1)M_1^6 - \gamma M_1^2(M_1^2-1)}{4(M_1^2-1)^2}\theta^2, \tag{12}$$

only the first term need be used when θ is small. The assumption that $M_1 \gg 1$ is not correct over some parts of the body, even for $M_\infty \gg 1$, so the hypersonic approximation to this relation should not be used.

The question of how an effective body contour can be found from the boundary-layer calculation must be considered. The displacement thickness is essentially a concept which satisfies the continuity relations. When waves reflect from a solid boundary with a boundary layer, the mechanism is not the same as for reflexion from a solid boundary without a boundary layer located at a distance of the displacement thickness from the actual boundary. Since no exact solution to this problem is available, and the disturbances are small, the assumption that the displacement thickness contour represents an effective body contour can be used as first approximation.

4. Calculation

Detailed calculations of the effect of the Reynolds number on the pressure distribution on a blunted flat plate have been made at $M = 11{\cdot}4$ for $\gamma = \frac{5}{3}$, since experimental results were available for this case. The pressure distribution and

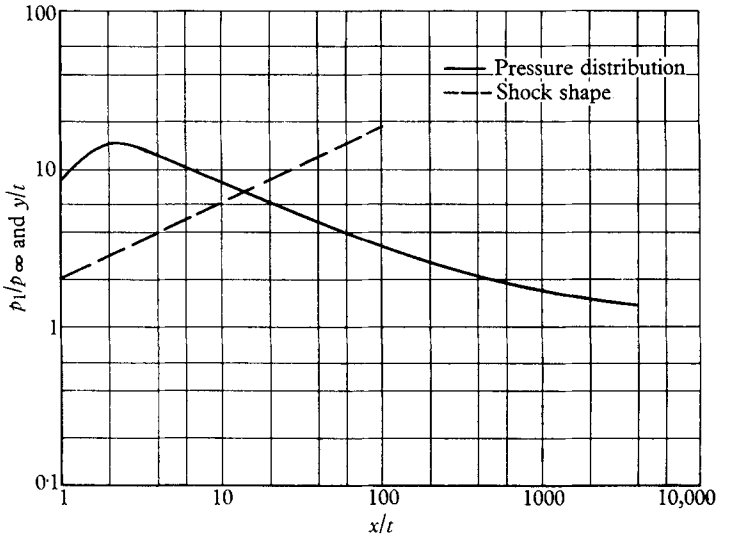

FIGURE 4. Inviscid pressure distribution and shock shape based on experiments at high Re_t; $M = 11{\cdot}4$.

shock shape shown in figure 4 are taken from the experimental results for the high Reynolds number case. The first step in the analysis is to calculate the growth of the boundary layer in this pressure field. For the initial calculation, the entropy on the outside of the boundary layer will be assumed to be that behind a normal shock. With the assumption for the P_1 against x/t relation given in figure 4, λ can be evaluated as a function of x/t by equation (11). Also δ^*/δ_S is a function of the shape of the boundary-layer profile and can be found by integrating the velocity-density distribution:

$$\frac{\delta^*}{\delta_S} = \frac{2}{7} + \frac{\frac{1}{2}(\gamma-1)M_\infty^2(u_1/u_\infty)^2}{1+\frac{1}{2}(\gamma-1)M_\infty^2(1-u_1^2/u_\infty^2)}(0{\cdot}3950 + 0{\cdot}02116a_2 - 0{\cdot}000622a_2^2) + \tfrac{2}{105}a_2. \tag{13}$$

Therefore, from the definition of λ,

$$\frac{\delta^*}{t}(\mathrm{Re}_t)^{\frac{1}{2}} = \frac{\delta^*}{\delta_S}(\lambda C)^{\frac{1}{2}}, \tag{14}$$

where λ and δ^*/δ_S are both functions of x/t. This relation is shown as a function of x/t in figure 5. The pressure distribution caused by the effective viscous distortion of the body can be found by setting the slope of the displacement thickness curve equal to θ in the first term of equation (12). If this is done, there follows

$$\frac{\Delta p}{p_{\mathrm{in}}} = \frac{\gamma M_1^2}{(M_1^2-1)^{\frac{1}{2}}}\frac{d\delta^*}{dx} = \frac{\gamma M_1^2}{(M_1^2-1)^{\frac{1}{2}}}\frac{Z}{(\mathrm{Re}_t)^{\frac{1}{2}}}, \quad Z = \frac{d}{d(x/t)}\left[\frac{\delta^*}{\delta_S}(\lambda C)^{\frac{1}{2}}\right], \tag{15}$$

where Z is a function only of x/t. The quantity $\Delta p(\mathrm{Re}_t)^{\frac{1}{2}}/p_{\mathrm{in}}$ is shown plotted as a function of x/t in figure 6.

The static pressure on the flat plate can be written

$$\frac{p}{p_\infty} = \frac{p_{\mathrm{in}}}{p_\infty}\left(1+\frac{\Delta p}{p_{\mathrm{in}}}\right).$$

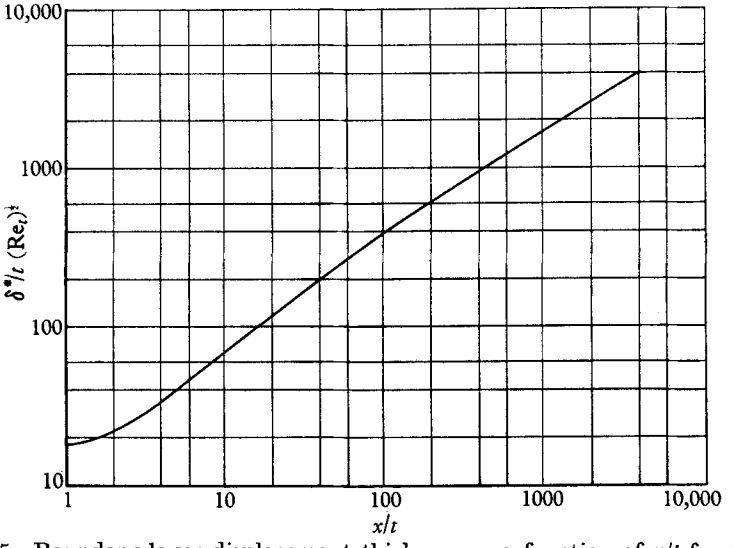

FIGURE 5. Boundary-layer displacement thickness as a function of x/t for constant total pressure on the outside of the boundary layer.

Therefore, if the experimental values of p/p_∞, measured as a function of x/t and Re_t, are divided by $1+\Delta p/p_{\mathrm{in}}$, calculated as a function of x/t, the result should be p_{in}/p_∞, which is only a function of x/t. This has been done and the results are shown in figure 7. The function p_{in}/p_∞ from figure 4, on which the calculation was based, is also shown in this figure. The discrepancy between these two curves indicates that there is some viscous correction even for the large Re_t on which the curve of figure 4 was based; however, the difference which would be caused by this error in the calculation of $\Delta p/p_{\mathrm{in}}$ is slight. It should be noted that data are available only at the high x/t values for low Fe_t and the low x/t values are for high Re_t.

Very far from the leading edge the effects of the viscous and inviscid leading edge phenomena must disappear. In the present solution, the pressure returns to

free stream value but the Mach number and entropy at the edge of the layer do not. This result is incorrect especially at high x/t. The entropy can be found for any Re_t by considering the mass in the boundary layer and tracing the stream line back to the point where it crossed the shock wave. The entropy at the outside of the boundary layer will be a function of both x/t and Re_t, so a new calculation

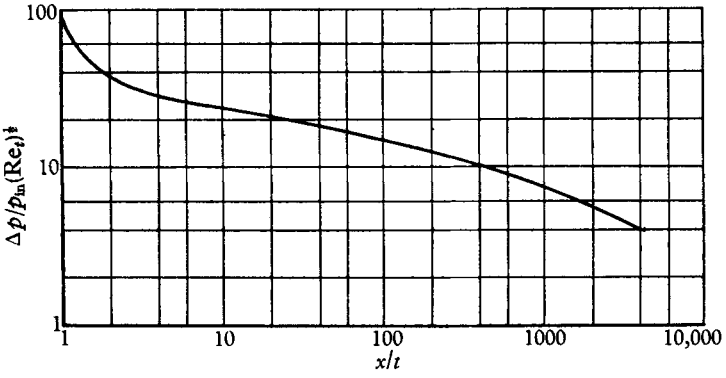

FIGURE 6. Pressure increment caused by boundary-layer displacement thickness as a function of x/t for constant total pressure on the outside of the boundary layer

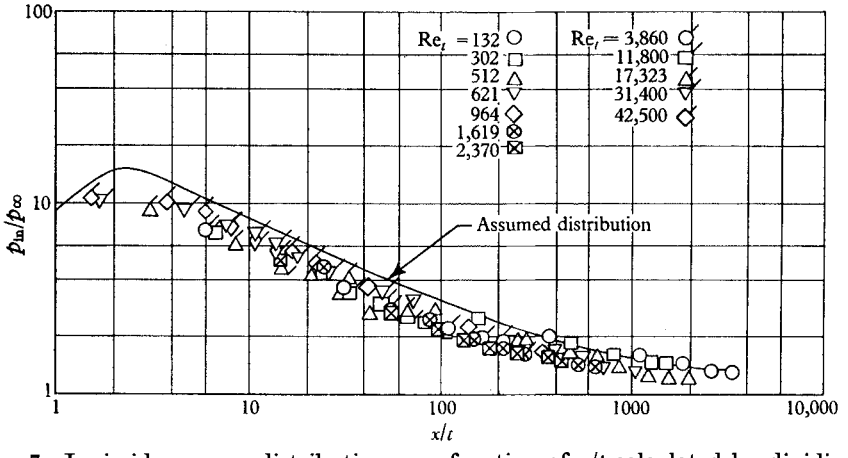

FIGURE 7. Inviscid pressure distribution as a function of x/t calculated by dividing the measured pressure distributions by the calculated viscous correction for constant total head on the outside of the boundary layer.

must be made for each value of Re_t. Such calculations have been made for $\mathrm{Re}_t = 132$ and 2370. The shock shape given in figure 4 is used for these calculations. As has been previously pointed out, the shock shape in the region of the leading edge is practically independent of Re_t. Once $G(x/t, \mathrm{Re}_t)$ is established, equation (11) may be evaluated and a new λ determined. It should be noted that the change in G will also change the value of u_1, T', δ^* and $\Delta p/p_1$. A new curve of p_{in}/p_∞ may then be plotted, based on the consideration of variable G along the edge of the boundary layer. This result is shown in figure 8. The points for low Re_t are changes from the constant G results, and correlate better with the points at higher Re_t. Since the experimental results at the same x/t and over the full

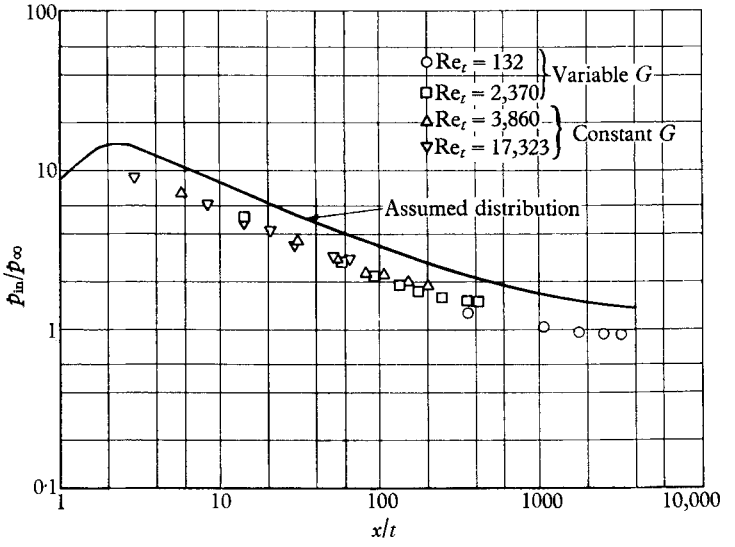

FIGURE 8. Inviscid pressure distribution as a function of x/t, calculated by dividing the measured pressure distributions by the calculated viscous correction for the corrected values of total head on the outside of the boundary layer.

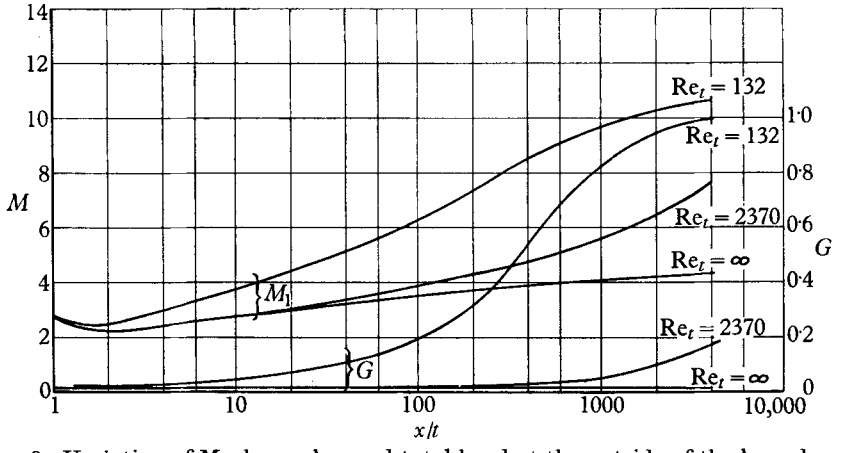

FIGURE 9. Variation of Mach number and total head at the outside of the boundary layer as a function of x/t at various Re_t.

Re_t range are not available, it is hard to make a good comparison. The value of G and M_1 for the various Re_t are shown in figure 9. G and M_1 do approach the free stream values at high x/t and low Re_t as expected. If more accurate results are required, these may be obtained by using the values of pressure and entropy found by the first calculation, to recalculate the whole system.

Correlation with previous work

Lees & Probstein (1952) investigated the viscous part of this problem without recognizing the important inviscid effect of the leading edge. Since the inviscid effect becomes unimportant at high x/t and low Re_t, their work should be a special

case of the present solution. For $G = 1$ and $p_{in}/p_\infty = 1$, the present solution gives

$$\delta^*/x = 1{\cdot}21(\gamma - 1)\, M_\infty^2\, (C/\mathrm{Re}_x)^{\frac{1}{2}}$$

for the growth of the boundary layer. Lees & Probstein obtained a result similar in all respects to this except that the numerical coefficient 1·21 is replaced by 1·197. This slight difference is caused by the different techniques used in solving the boundary-layer equations. The experiments reported by Kendall (1957) agree with the present theory if $p_{in}/p_\infty = 1$ and $G = 1$. These assumptions are probably correct for the case of low M and Re_t, since the x/t parameter is not necessary to correlate the results of this experiment. The present theory provides a means of correlating the results of Kendall (1957) made in a hot-air tunnel at a Mach number of about 6 and those obtained in the Princeton helium tunnel at Mach numbers between 11 and 15.

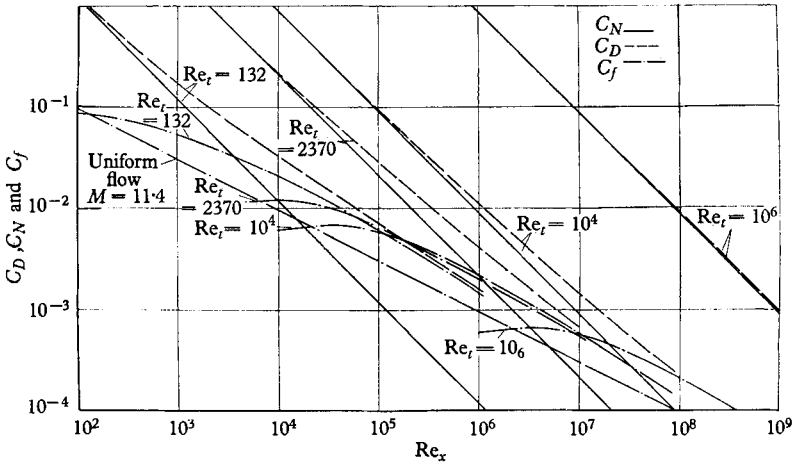

FIGURE 10. Friction drag, nose drag, and total drag for a blunted flat plate at various Re_t; $M = 11{\cdot}4$.

Skin friction and Drag

Since the present solution is for the adiabatic case, no direct information of heat transfer can be obtained, but the friction and drag forces may be calculated. The average skin friction parameter has been calculated on the basis of the boundary layer solutions found in this analysis. The results are presented in figure 10 as a function of Re_t and Re_x. The results for $\mathrm{Re}_t = 132$ and $\mathrm{Re}_t = 2370$ are for the solution which takes into account the variation of G with x/t. The curves for $\mathrm{Re}_t = 10^4$ and 10^6 are for the solution with constant G, since G shows very little variation at these Reynolds numbers over the x/t range of this figure. It is interesting to note that the curves for the various Re_t form an envelope and give fairly uniform values as a function of Re_x over most of the range. The values of C_f calculated by conventional boundary-layer theory (Van Driest 1952), leaving out the change of inviscid flow conditions caused by both the leading edge and the boundary layer, are also shown. The present results give skin friction values of the order of twice the results of conventional theory.

In addition to the friction drag, there is the pressure drag on the nose of the plate. Since the details of the nose affect the flow about the whole body, it is not

reasonable to consider just the skin friction term. The pressure drag is also presented in figure 10. For the low Re_t case ($\mathrm{Re}_t = 132$), the nose drag is smaller than the skin friction drag for $\mathrm{Re}_x > 4 \times 10^3$. For high Re_t, the nose drag predominates up to Re_x of the order of 10^7. The drag coefficients are only for one side of the plate and the pressure drag on one half the blunt nose. The full drag would be twice these values for a symmetrical body. The total drags are also shown on this figure as the sum of the pressure and friction drags.

5. Discussion

These calculations show that by including the effect of the finite thickness of the leading edge, it is possible to derive a theory which accounts for the observed Reynolds number effects found for hypersonic flow about flat plates. Even down to very thin leading edges, the flat plate does not approach the infinitely thin flat plate. The flow conditions are shown to depend on the distance from the leading edge in terms of leading-edge thickness and the Reynolds number.

Some previous theoretical work had treated a strong interaction region where the pressure changes caused by the viscous forces are much larger than the inviscid pressures. If the effects of finite leading-edge thickness are considered, there need be no such region. The present method can be used over the entire body. The inclusion of the stagnation point flow, which must occur in any real case, allows a boundary layer with a finite initial rate of growth which need not cause large pressure changes. The strong interaction region only occurs at low values of Re_t where the growth of the boundary layer is rapid. An understanding of this flow picture eliminates many of the difficulties in treating the nose region which were encountered in the previous work.

The present analysis is a rough calculation designed to show the effects of the various significant parameters. Unfortunately, it was necessary to use numerical techniques to solve the boundary layer equations; however, an analytic solution cannot be expected until it is possible to solve the inviscid blunt-nosed problem so that the viscous solution need not be based on empirical results. The results presented are for the restricted case of $M = 11{\cdot}4$ and $\gamma = \frac{5}{3}$. These values were chosen to match the available data. Calculations over the full range of Mach and Reynolds numbers have not been attempted. This technique can be used to calculate the viscous effect for any case in which the inviscid solution is known and the viscous correction can be considered a perturbation on the inviscid solution. The method can be applied to any two-dimensional plane or axially symmetric body once the basic inviscid pressure distribution is known. For plane two-dimensional bodies, the only change would be in the basic inviscid pressure distribution. For axially symmetric bodies, the boundary-layer solution would be modified to include the effect of the change of radius.

6. Conclusions

1. The Reynolds number effects on the pressure distribution and flow parameters about a body in hypersonic flow can be predicted by conventional boundary-layer theory once the inviscid flow is known.

2. There is no conceptual difficulty in analysing the flow near the leading edge if the real case of a finite leading edge is considered.

3. The skin friction on the surface of a flat plate is of the order of twice the skin friction calculated by conventional flat plate boundary-layer theory. The skin friction is relatively independent of Re_t, but the total drag increases rapidly with Re_t.

The present study is part of a programme of theoretical and experimental research on hypersonic flow being conducted by the Gas Dynamics Laboratory, James Forrestal Research Center, Princeton University, Wright Air Development Center of the United States Air Force, under Contract No. AF 33(616)–2547, with Fred L. Daum as project engineer.

REFERENCES

BECKER, J. V. 1950 Results in recent hypersonic and unsteady flow research at the Langley Aeronautical Laboratory. *J. Appl. Phys.* **21**, 622.

BERTRAM, M. H. 1952 An approximate method of determining the displacement effects and viscous drag of laminar boundary layers in two-dimensional hypersonic flow. *Nat. Adv. Comm. Aero., Wash., Tech. Note*, no. 2773.

BERTRAM, M. H. 1954 Viscous and leading edge thickness effects on the pressures on the surface of a flat plate in hypersonic flows. *J. Aero. Sci.* **21**, 430.

BOGDONOFF, S. M. & HAMMITT, A. G. 1954 The Princeton helium hypersonic tunnel and preliminary results above $M = 11$. *Princeton University Aero. Eng. Rep.* no. 260. (Also published as *WADC TR* 54–124.)

BOGDONOFF, S. M. & HAMMITT, A. G. 1956 Fluid dynamic effects at speeds from $M = 11$ to 15. *J. Aero. Sci.* **23**, 108.

CHANG, H. K. & PALLONE, A. J. 1956 Inviscid leading edge effect in hypersonic flow. *J. Aero. Sci.* **23**, 700.

HAMMITT, A. G. & BOGDONOFF, S. M. 1956 Hypersonic studies of the leading edge effect on the flow over a flat plate. *J. Amer. Rocket Soc.* **26**, 241.

HAMMITT, A. G., VAS, I. E. & BOGDONOFF, S. M. 1956 Leading edge effects on the flow over a flat plate at hypersonic speeds. *Princeton University Aero. Eng. Rep.* no. 326. (Also published as *WADC TN* 55–537.)

KENDALL, J. M. 1957 An experimental investigation of leading edge shock wave boundary layer interaction at $M = 5{\cdot}8$. *J. Aero. Sci.* **24**, 47.

KUO, Y. H. 1953 On the flow of an incompressible viscous fluid past a flat plate at moderate Reynolds numbers. *J. Math. Phys.* **32**, 83.

LEES, L. 1952 On the boundary layer equations in hypersonic flow and their approximate solutions. *Princeton University Aero. Eng. Rep.* no. 212.

LEES, L. 1954*a* Hypersonic viscous flow over an inclined wedge. *J. Aero. Sci.* **20**, 794.

LEES, L. 1954*b* Hypersonic influence of the leading edge shock wave on the laminar boundary-layer at hypersonic speeds, *GALCIT TR*, no. 1.

LEES, L. & KUBOTA, T. 1956 Inviscid hypersonic flow over blunt-nosed slender bodies. *J. Aero. Sci.* **123**, 195.

LEES, L. & PROBSTEIN, R. F. 1952 Hypersonic viscous flow over a flat plate. *Princeton University Aero. Eng. Rep.* no. 195.

LI, TING-YI & NAGAMATSU, H. 1953 Shock wave effects on the laminar skin friction of an insulated flat plate at hypersonic speeds. *J. Aero. Sci.* **20**, 345.

LI, TING-YI & NAGAMATSU, H. 1955 Hypersonic viscous flow on a non-insulated flat plate. *GALCIT Report*, no. 25.

MORDUCHOW, M. & CLARKE, JOSEPH H. 1952 Method for calculation of compressible laminar boundary-layer characteristics in axial pressure gradient with zero heat transfer. *Nat. Adv. Comm. Aero., Wash., Tech. Note,* no. 2784.

PAI, SHIH-I 1953 On strong interaction for the hypersonic boundary layer on inclined wedge. *J. Aero. Sci.* **20**, 796.

SHEN, S. F. 1952 An estimate of viscosity effect in hypersonic flow over an insulated wedge. *J. Math. Phys.* **31**, 192.

VAN DRIEST, E. F. 1952 Investigation of laminar boundary layer in compressible fluids using the Croco method. *Nat. Adv. Comm. Aero., Wash., Tech. Note,* no. 2597.

VAS, I. E. 1957 An experimental investigation of the pressure on a thin flat plate at hypersonic speeds. *Princeton University Aero. Eng. Rep.* no. 377. (Also published as *WADC TN* 57–104.)